PAPER

Check for updates

Screening the functions of modified rice straw biochar for adsorbing manganese from drinking water†

Jie Zhao,[ab] Zhi-Long Ye, ID *[a] Xiaofang Pan,[a] Guangjing Cai[a] and Jiani Wang[a]

The seasonal out-of-limit of manganese ions (Mn^{2+}) in the drinking water reservoirs is an intractable problem to water supply, which can pose a threat to the human health. In this study, the removal of Mn^{2+} by using pristine (BC), pre-alkali (Pre-BC) and post-alkali (Post-BC) modified biochar originating from rice straw was investigated. The maximum adsorption capacities obtained for BC, Pre-BC, and Post-BC were 20.59, 28.37, and 8.06 mg g^{-1}, respectively. The Langmuir isotherm model and the pseudo-second-order kinetic model were suitable fitting models to describe the adsorption process. The investigation of adsorption functions was carried out that revealed that the predominant forces were precipitation and cation exchange with the proportions of 43.38–69.15% and 38.05–55.79%, respectively. With regard to precipitation, Mn(II) particles (Al–Si–O–Mn and $MnCO_3$) and insignificantly oxidized insoluble Mn(IV) particles (MnO_2) were formed on the biochar surface. Alkali and alkaline earth metals facilitated the behavior of cation exchange, where the primary contributing ions for cation exchange were Na$^+$, Mg^{2+} and Ca^{2+} during the adsorption process. These outcomes suggest that alkali pre-treated modification of biochar is practical for the application of manganese pollution control in lakes and reservoirs.

Introduction

Lakes and reservoirs are the main water sources for agriculture, industry, and municipality. However, seasonal out-of-limit levels of manganese in lakes and reservoirs have become an intractable problem in many areas of the world, threatening the safe water supply. Due to the existence of seasonal hypolimnion anoxia (especially in summer) in the lakes and reservoirs,[1] dissolved oxygen at the bottom of the water body might decrease dramatically, which would lead to the release of Mn^{2+} from the sediments to the upper aquifer driven by the manganese-reducing micro-organisms.[2] This would bring a security threat to the operation of the drinking water supply. Mn^{2+} content exceeding the limit in drinking water can be a potential risk to human health by causing chronic poisoning. Excessive intake of Mn^{2+} would cause symptoms such as sleep disorders, salivation, confusion in speech and slow movement, which would damage the human nervous system, especially in children.[3] Besides, excessive levels of Mn^{2+} would cause aesthetic and operational

problems during the transportation of water supply such as laundry stains and pipe clogging, respectively.[4] Therefore, many countries have developed Mn limit standards for water supply. The United Nations Drinking Water Quality Standard stipulates that the limit of Mn^{2+} should be under 0.05 mg L^{-1},[3] and some water utilities even require restrictions of 0.02 mg L^{-1} to enhance the water quality.[1] Hence, it is important to develop feasible technologies to remediate Mn^{2+} pollution in lakes and reservoirs.

Some technologies, including catalytic oxidation,[4] biological oxidation,[5] and adsorption,[6] have been tested to reduce manganese contamination in water bodies. Due to relative high efficiency and easy operation, the application of adsorption is promising. At present, typical adsorbent materials including activated carbon,[6] carbon nanotubes[7] and nanocomposites[8] are reported. Benefiting from the advantages of low cost and high adsorption performance, the implementation of biochar as an adsorbent for heavy metals is a promising option in environmental remediation.[9,10] The conversion of agricultural and forestry waste into biochar for environmental remediation application is an effective way to reuse waste resources, which could effectively improve the efficiency of waste utilization and relieve the pressure of resource scarcity.[11]

Biochar, as the product obtained from biomass pyrolysis under an oxygen-limited environment, possesses multidimensional pore structures, abundant functional groups, and complex surface properties.[12,13] Normally, biochar directly

[a]*Key Laboratory of Urban Pollutant Conversion, Institute of Urban Environment, Chinese Academy of Sciences, No. 1799 Jimei Road, Xiamen City, Fujian 361021, China. E-mail: zlye@iue.ac.cn; jzhao@iue.ac.cn*

[b]*College of Life Sciences, Fujian Agriculture and Forestry University, Fuzhou, 350002, China*

† Electronic supplementary information (ESI) available. See https://doi.org/10.1039/d2ra01720b

prepared from conventional agriculture and forestry wastes has limited adsorption capacity for certain heavy metals, which is due to insufficiently active functional groups and low selectivity.[14] For instance, the pristine biochar has a limited adsorption capacity for the removal of arsenic and cadmium.[15] Studies have been conducted to enhance biochar adsorption capacity through surface modification.[16–18] It has been reported that alkali modification was available to improve the specific surface area and functional groups of biochar, thereby increasing its adsorption performance.[19] As for the removal of heavy metals, alkali modification by using NaOH or KOH is recommended, which can increase Na composition and oxygen-containing functional groups toward biochar and therefore improve the adsorption capacity on heavy metals.[20] Peter et al.[21] reported that NaOH-treated softwood biochar could homogenously distribute Na^+ on the surface of biochar and thereafter improved the adsorption capacity 22 times higher than that of the unmodified biochar for Cu^{2+} removal. For the removal of Mn^{2+} from lakes and reservoirs, limited works have been reported on the relevant issue.

Presently, regarding biochar removing Mn^{2+}, there is limited information available to describe adsorption functions. An et al.[22] reported that the possible adsorption mechanism was the formation of $MnCO_3$ and $-COOMn^+$, which were generated during Mn^{2+} adsorption by pomelo peel biochar. Recent studies revealed that the main adsorption functions responsible for heavy metal adsorption could be precipitation, metal cation exchange, complexation with oxygen-containing functional groups, and chelation with π electrons.[23–25] For different heavy metals, the interaction mechanisms between biochar and the adsorbates could be different. For instance, a recent study revealed that nanosized MgAl-layered double hydroxide-coated rice husk biochar could promote its adsorption capacity on Cu^{2+} and Cd^{2+} via precipitation with CO_3^{2-} and SO_4^{2-} and ion exchange with Mg^{2+}.[26] Iamsaard et al.[27] found that the predominant functions of pineapple leaf biochar adsorbing Ni^{2+}, Zn^{2+} and Cu^{2+} were cation exchange to metal ions such as Na^+, Mg^{2+}, K^+, Ca^{2+} and surface complexation with functional groups such as COOH, C–O, C–H, and C–C bonds. Hence, in order to effectively remove Mn^{2+} from the water body, a comprehensive investigation of the adsorption behavior by modified biochar is necessary.

In this study, rice straw biochar was prepared and modified by using alkali pre-treated and post-treated modification, respectively, so as to investigate the performance of manganese removal from the water supply. The adsorption isotherm and kinetics were investigated and the functional mechanisms were clarified by using a combination of different analyses. The research outcomes were expected to provide methodological support for controlling manganese endogenous pollution for a safe drinking water supply.

Materials and methods

Biochar preparation and modification

Raw rice straw was purchased from Lianfeng Agricultural Products Deep Processing Company Limited, China. The raw

biomass was first dried at 105 °C and then pyrolyzed at 600 °C for 2 hours under a nitrogen atmosphere in a quartz tube furnace (OTF-1200X, Hefei Crystal Materials Technology Co., Ltd, China). After the temperature was reduced, the generated biochar (BC) was ground to powder and passed through a 40 mesh sieve.

With regard to biochar modification, methods including pre- and post-modification processes are conducted. The pre-alkali modified biochar (Pre-BC) was prepared by treating raw biomass with alkali before the carbonization method, which referred to the method proposed by An et al.[22] The details are described in the following steps: raw biomass was initially mixed with 2.5 M NaOH solution with a solid-to-liquid ratio at 1 : 10 (w/v), and then subjected to drying at 80 °C, followed by pyrolysis like BC. After that, excess alkali was washed with deionized water and dried for the experiments. Regarding the post-alkali modified biochar (Post-BC), the alkali treatment was after the pyrolysis. The prepared BC was directly mixed with 2.5 M NaOH solution at the same mixing ratio, then washed with deionized water, and dried to obtain Post-BC.

In order to distinguish the different adsorption functions of biochar on Mn^{2+} removal, the pristine biochar, and modified biochar were demineralized through rinsing steps using 1 M HCl solution, followed by washing with deionized water until the pH was constant. Previous studies have suggested that this approach did not bring about significant changes in the oxygen-containing functional groups on the surface of the biochar, which could reveal that the functions of complexation and cation-π with heavy metals were contributed by the demineralized biochar.[23,25]

Experimental procedure

Adsorption isotherm and kinetics. Batch adsorption experiments were conducted to investigate the different adsorption behavior between unmodified and modified biochar. As for the experimental adsorption isotherms, a certain amount of biochar was added to the solutions containing different Mn^{2+} concentrations (1–200 mg L^{-1}). Then, the solutions were subjected to agitation at 150 rpm for 12 h, and the temperature was controlled at 25 °C. After the agitation, the supernatant was filtered through a 0.45 μm Millipore membrane filter for analyses. Regarding the test of adsorption kinetic, 0.4 g biochar was dosed into the solution with 50 mg L^{-1} Mn^{2+} in the conical flasks, and samples were periodically withdrawn for measurement. All the tests were conducted in triplicate.

The adsorption isotherm was evaluated through the equations of Langmuir (eqn (1)), Freundlich (eqn (2)) and Temkin equation (eqn (3)), as described below.

$$Q_e = \frac{Q_{max} K_L C_e}{1 + K_L C_e} \tag{1}$$

$$Q_e = K_F C_e^{\frac{1}{n}} \tag{2}$$

$$Q_e = \frac{RT}{b_T} \ln(K_T C_e) \tag{3}$$

where C_e (mg L^{-1}) and Q_e (mg g^{-1}) are the concentration of Mn^{2+} and adsorption capacity at equilibrium conditions, respectively. Q_{max} (mg g^{-1}) is the theoretical maximum adsorption capacity of the Langmuir model. K_L, K_F, and K_T are the rate constants of the Langmuir, Freundlich, and Temkin models, respectively. n is the degree of nonlinearity between the adsorbent and adsorbate for the rate constant of the Freundlich equation.

The adsorption kinetics was assessed using equations of Lagergren's pseudo-first-order (eqn (4)), pseudo-second-order (eqn (5)), and Elovich (eqn (6)), respectively.

$$Q_t = Q_e(1 - e^{-k_1 t}) \qquad (4)$$

$$Q_t = \frac{k_2 Q_e^2 t}{1 + k_2 Q_e t} \qquad (5)$$

$$Q_t = \frac{1}{\beta}\ln(1 + \alpha\beta t) \qquad (6)$$

where Q_t (mg g^{-1}) is the adsorption capacity at time t. k_1 (min^{-1}) and k_2 (g mg^{-1} min^{-1}) are the rate constants of pseudo-first-order, and pseudo-second-order, respectively. α (mg g^{-1} min^{-1}) and β (mg g^{-1}) are the Elovich rate constants referring to adsorption–desorption processes, respectively. b (mg g^{-1}) is the ordinate intercept.

Adsorption functions. According to the literature, biochar can remove heavy metals through different functions, including surface precipitation (Q_{pre}), metal cation exchange (Q_{exc}), complexation with oxygen-containing functional groups (Q_{com}), and coordination of Mn^{2+} with π electrons ($Q_{c\pi}$).[23–25] In this section, the functions of modified biochar adsorbing Mn^{2+} were investigated through a series of subsequent experiments. According to the previous experiments on adsorption isotherms and kinetics, an initial Mn^{2+} concentration of 50 mg L^{-1} was selected for this part. 0.4 g raw biochar or demineralized biochar were mixed with 200 mL of 50 mg L^{-1} Mn^{2+} solution and then was subjected to agitation at 150 rpm for 12 h. After the agitation, the supernatant was filtered through a 0.45 μm Millipore membrane for cationic measurement. Deionized water without Mn^{2+} was used as the control blank to calculate the cation exchange capacity. The contribution of different functions of biochar adsorbing heavy metal was examined by using the methodology, as described in the previous study.[23] The detailed steps were:

(1) Q_{cm} was comprised of Q_{pre} and Q_{exc}, which were determined by the difference in Mn^{2+} adsorption capacities between untreated and demineralized biochar. Q_{exc}, representing the function of cation exchange (Na$^+$, Mg^{2+}, K$^+$, and Ca^{2+}), was calculated using the net release of cations during the adsorption progress from untreated biochar. The adsorption capacity of Q_{pre} was determined by the difference between Q_{cm} and Q_{exc}. The values of Q_{cm}, Q_{pre} and Q_{exc} were determined by the following equations:

$$Q_{cm} = Q_e - Q_{de} \times Y \qquad (7)$$

$$Q_{exc} = \sum Q_i \qquad (8)$$

$$Q_{pre} = Q_{cm} - Q_{exc} \qquad (9)$$

where Q_{de} (mg g^{-1}) is the adsorption capacity of demineralized biochar. Q_i (mg g^{-1}) is the net amount of Mn^{2+} adsorption capacity by the cation exchange capacity of Na$^+$, Mg^{2+}, K$^+$, and Ca^{2+}, respectively. Y is the residual ratio of biochar after demineralization.

(2) Q_{com} is caused by ion exchange between the protons (H$^+$) of oxygen-containing functional groups and Mn^{2+}, which resulted in the release of H$^+$ into the solution during the adsorption process. Therefore, Q_{com} was determined by the pH change before and after the adsorption of the demineralized biochar. $Q_{c\pi}$ was calculated by the Q_{com} values deducted from the Q_{de} values. The values of Q_{com} and $Q_{c\pi}$ were determined by the following equations.

$$Q_{com} = Q_{pH} \times Y \qquad (10)$$

$$Q_{c\pi} = Q_{de} \times Y - Q_{com} \qquad (11)$$

Analytical methods

The pH value was measured using a pH meter (Rex PHS-3C, China). The ash content was determined according to the standard (GB/T 12496.3-1999, China). Elemental contents of C, H, O, and N were determined using an elemental analyzer (Vari Macro CHNS–O–Cl, Germany), and inorganic elemental contents of Na, Mg, K, Ca, Al, Si, P, and Mn were determined using an X-ray fluorescence spectrometer (XRF, Axios-MAX, Netherlands). The specific surface area, average pore size, and pore volume were assayed using a Brunauer–Emmett–Teller (BET) analyzer (ASAP 2020M+C, America). The morphology of biochar was observed using a field emission scanning electron microscope and equipped with an X-ray energy spectrometer (SEM-EDX, S-4800, Japan). The element composition and valence were measured using an X-ray photoelectron spectrometer (XPS, Axis Supra, England) and analyzed using the Thermo Avantage v5.9922. The concentration of cations was assayed using an inductively coupled plasma emission spectrometer (ICP-OES, Optima 7000DV, America).

Results and discussion

Physicochemical properties of biochar

The physicochemical properties of BC, Pre-BC, and Post-BC are displayed in Table 1. The sum content of C, H, O in the raw biochar and modified biochar ranged from 62.37% to 68.42%, which could provide a matrix for oxygen-containing functional groups (–OH, –COOH) and π electro donors (–C=C–, –C≡C–).[28] The atomic ratio of O/C and H/C did not display an obvious difference for the untreated and treated biochar, indicating that the alkali modification did not significantly change the structure of organic functional groups. FTIR spectra are shown in Fig. 1, the spectra of BC and Pre-BC showed similar profiles, which meant that the functional groups were not significantly changed by the alkali pretreatment. The FTIR spectrum of Post-

Table 1 Physicochemical properties of BC, Pre-BC, Post-BC

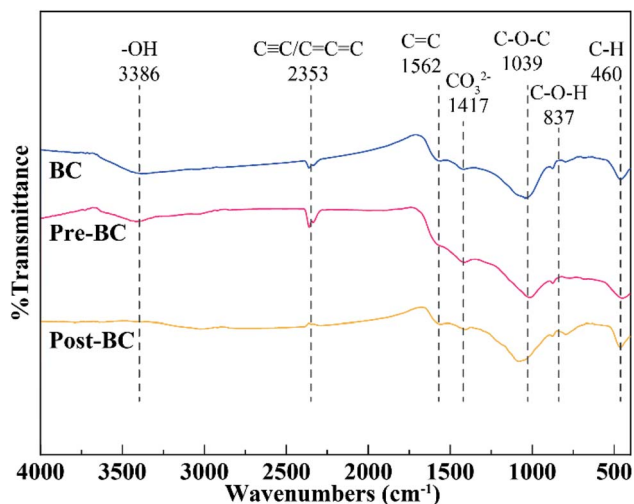| Biochar	BC	Pre-BC	Post-BC
C	46.97%	46.84%	50.71%
O	14.01%	13.28%	15.45%
H	2.19%	2.25%	2.26%
N	1.34%	0.27%	0.89%
Na	0.01%	0.05%	0.01%
Mg	0.11%	0.14%	0.14%
K	4.97%	0.25%	1.26%
Ca	2.27%	4.09%	2.55%
Al	0.28%	0.22%	0.22%
Si	4.03%	3.32%	3.28%
P	0.51%	0.17%	0.50%
Mn	0.75%	0.99%	1.18%
O/C	0.30	0.28	0.30
H/C	0.05	0.05	0.04
Ash	43.57%	44.68%	30.82%
S_{BET} (m^2 g^{-1})	3.76	110.16	84.83
Average pore size (nm)	11.06	4.60	5.87
V_{BJH} (cm^3 g^{-1})	0.02	0.15	0.14

Fig. 1 FTIR spectra of BC, Pre-BC, and Post-BC.

BC was obviously changed at 3386, 2353, 1417, and 1039 cm^{-1}, representing the functional groups of –OH, C≡C/C=C=C, CO_3^{2-}, and C–O–C, respectively.[19,29,30] The ash content of Post-BC (30.82%) was remarkably lower than those of Pre-BC (44.68%) and BC (43.57%). This could be ascribed to the release of internal volatile substances during the carbonization of biochar,[29] however, the alkali post-treatment made part of the ash wash away. The main mineral compositions in ash are listed in Table 1, which suggested that different interactions occur, such as cation exchange and precipitation, between biochar and adsorbate.[31] Details will be discussed in the section below.

Table 1 shows that the specific surface area, average pore size, and pore volume of alkali-modified biochar, coupled with the N$_2$ adsorption/desorption isotherm (Fig. S1†), changed significantly. The specific surface areas of Pre-BC (110.16 m^2

g^{-1}) and Post-BC (84.83 m^2 g^{-1}) were about 29.30 and 22.56 times higher than that of BC (3.76 m^2 g^{-1}). The average pore size of Pre-BC and Post-BC decreased by 2.40 and 1.88 times, and the pore volume increased by 7.50 and 7.00 times. These results indicated the alkali modification could alter the porous structure from the macroscale to the mesoscale. The changes in the pore structure also could be observed in Fig. 2.

Adsorption performance

Adsorption isotherms. Fig. 3A shows the adsorption capacity and removal efficiency of Mn^{2+} at different initial concentrations. It was obvious that Pre-BC possessed the highest adsorption capacity with a value at 28.61 mg g^{-1}. BC displayed a higher adsorption performance than Post-BC. The results indicated that the alkali pre-treatment modified biochar could improve the affinity of biochar with Mn^{2+}. The experimental data were subjected to the equation regression, as shown in Fig. 3B–D. The calculated constant parameters and correlation coefficients of the adsorption isotherm model fitting are shown in Table 2. The regression outcome indicated that the Langmuir isotherm model was appropriate to describe the adsorption process, which implied that surface monolayer adsorption was predominant for the manganese ion adsorption by BC, Pre-BC, and Post-BC.[32] Accordingly, the theoretical maximum Mn^{2+} adsorption capacities of BC, Pre-BC, and Post-BC were 20.59, 28.37, and 8.06 mg g^{-1}, respectively. Besides, compared with the other biochar derived from woody (about 0.43 mg g^{-1}),[33] woody chips (about 1.58 mg g^{-1}),[6] and coffee grounds (about 19.6 mg g^{-1})[34] reported previously, Pre-BC showed an outstanding adsorption performance.
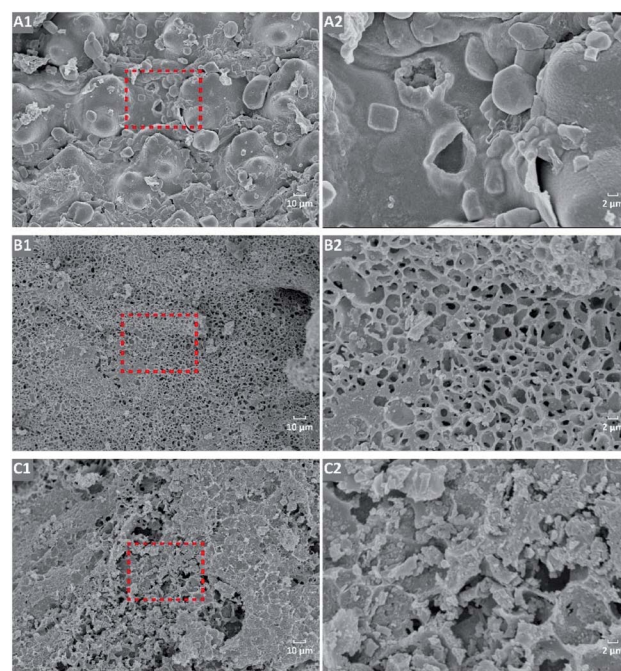

Fig. 2 SEM spectra of BC, Pre-BC, and Post-BC. *5.0k magnification times: (A1) of BC, (B1) of Pre-BC, (C1) of Post-BC; *20.0k magnification times: (A2) of BC, (B2) of Pre-BC, (C2) of Post-BC.
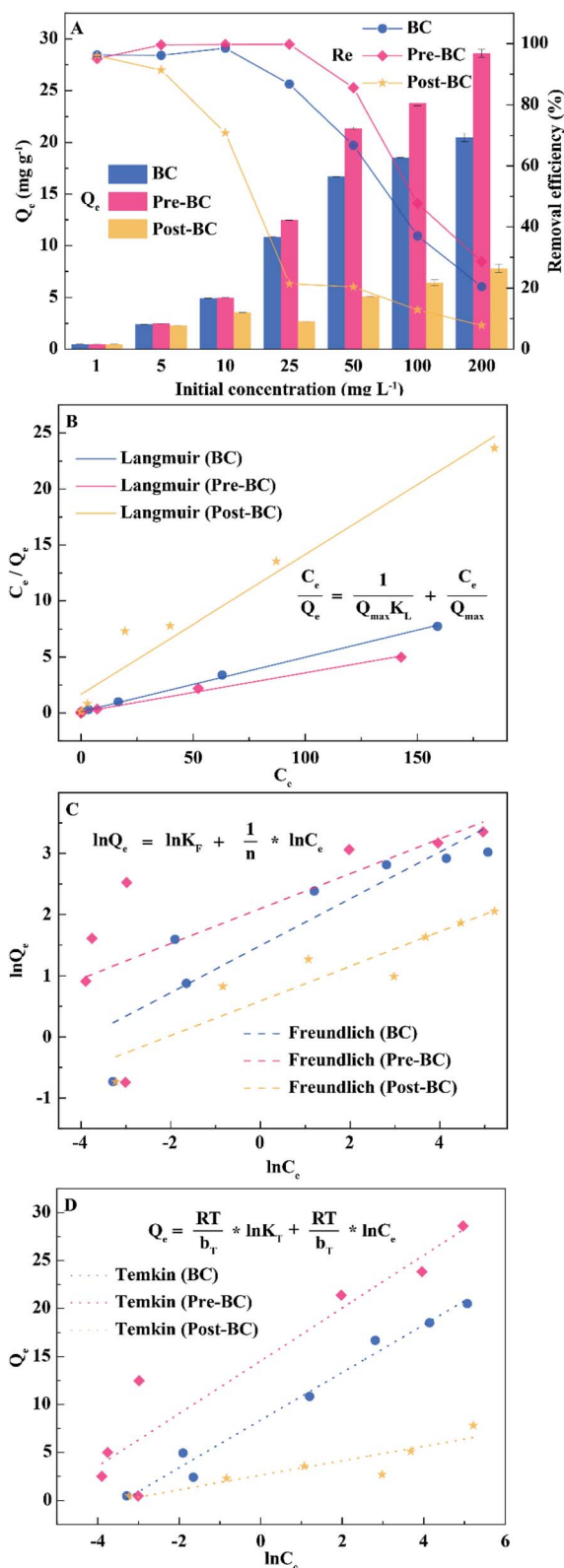
Fig. 3 Adsorption performance of Mn^{2+} under different initial concentrations and linear regression of the adsorption isotherms of BC, Pre-BC, and Post-BC. (A) adsorption performance of Mn^{2+}, (B) Langmuir model regression, (C) Freundlich model regression, (D) Temkin model regression.

Table 2 The fitting parameters of the adsorption isotherms for Mn^{2+} adsorption

Biochar		BC	Pre-BC	Post-BC
Langmuir	Q_{max}	20.59	28.37	8.06
	K_L	0.39	0.47	0.08
	R^2	0.998	0.994	0.947
Freundlich	K_F	4.441	8.133	1.800
	$1/n$	0.383	0.286	0.283
	R^2	0.783	0.457	0.833
Temkin	K_T	28.955	197.982	15.556
	RT/b_T	2.485	2.750	0.754
	R^2	0.978	0.877	0.791

Adsorption kinetics. Fig. 4 displays the adsorption capacity of Mn^{2+} at different contact times. In the first early-stage, Pre-BC exhibited the fastest adsorption efficacy with a capacity of 11.98 mg g^{-1}, accounting for 60.86% of the total amount (in the first minute), while the adsorption capacities of BC and Post-BC were 5.53 mg g^{-1} and 3.96 mg g^{-1} representing 30.48% and 75.00% of the total value, respectively. These results indicated that the alkali pre-treatment modified biochar could accelerate the Mn^{2+} adsorption. The experiment data were subjected to the equation regression, as shown in Fig. 4B–D. The calculated constant parameters and correlation coefficients are listed in Table 3. The values of R^2 indicated that the pseudo-second-order model was appropriate to describe the adsorption process. The pseudo-second-order model was proposed based on the assumption that the adsorption capacity is proportional to the number of active sites occupied on the adsorbent.[35] The rate-limiting step of the pseudo-second-order adsorption process was affected by valent forces by the sharing or the exchanging of electrons between the adsorbents and adsorbates.[36] This represented chemical adsorption behavior, which was related to the adsorption functions of precipitation, surface complexation and cation exchange.[19] This was consistent with the observed rapid adsorption at the initial stage in this study.[37] The better fitting of the Elovich model ($0.963 \leq R^2 \leq 0.988$) further described the chemisorption processes occurring on the heterogeneous surface of biochar.[38]

Quantification of the adsorption forces

The relative contributions of the different adsorption functions. The determination of different adsorption functions contributing to manganese removal was conducted as described in the fraction of "Adsorption functions" in "Experimental procedure". As shown in Fig. 5A, the predominant forces were cation exchange and precipitation, while surface complexation and chelation with cation-π had limited contribution to the adsorption capacities. The amount of precipitated manganese in BC, Pre-BC, and Post-BC were 11.24, 13.65, and 2.29 mg g^{-1}, which accounted for 61.95%, 69.35%, and 43.38% of the total removal amount, respectively. This outcome indicates that the precipitation was the key factor for Mn^{2+} adsorption. The cation exchange capacities for BC, Pre-BC, and Post-BC were 6.90, 5.83, and 2.84 mg g^{-1}, and the occupation
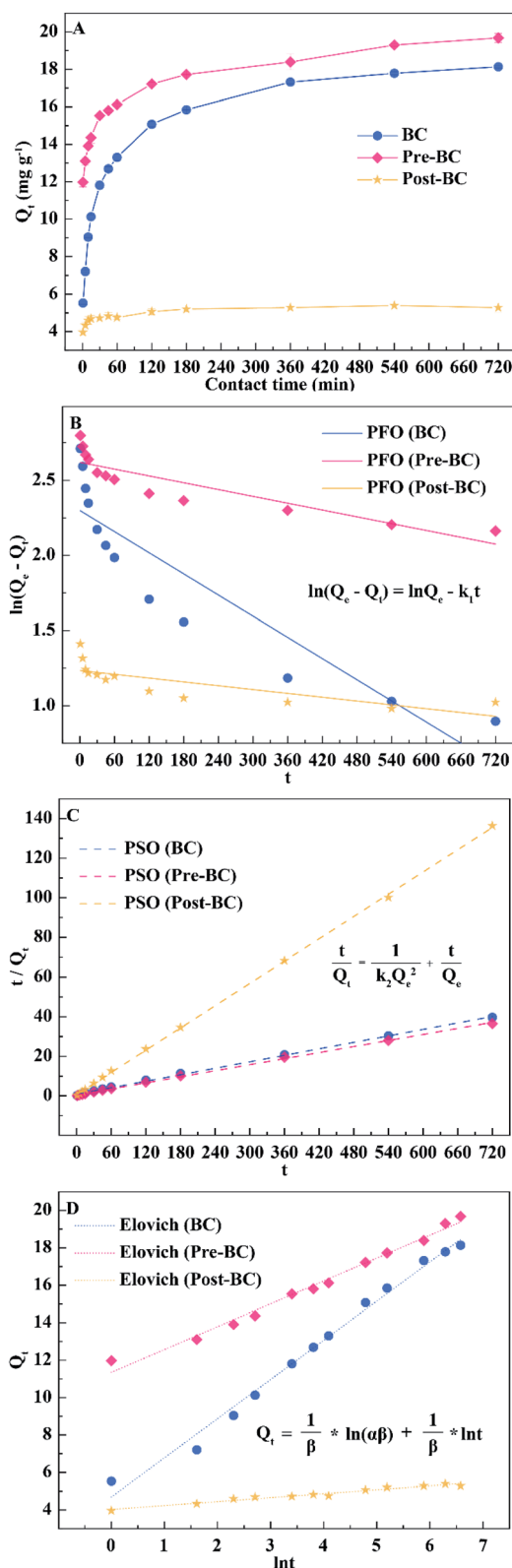
Fig. 4 Adsorption capacity of Mn^{2+} at different contact times and linear regression of adsorption kinetics by BC, Pre-BC, and Post-BC. (A) adsorption capacities of Mn^{2+}, (B) pseudo-first-order (PFO) model regression, (C) pseudo-second-order model (PSO) regression, (D) Elovich model regression.

Table 3 The fitting parameters of the adsorption kinetic for Mn^{2+} adsorption

Biochar		BC	Pre-BC	Post-BC
Pseudo-first-order	k_1	0.002	7.570	4.244
	R^2	0.814	0.770	0.571
Pseudo-second-order	k_2	0.003	0.005	0.057
	R^2	0.999	0.999	1.000
Elovich	α	19.649	13363.918	44030796.643
	β	0.478	0.820	4.762
	R^2	0.988	0.986	0.963

percentages of the total adsorption capacity were 38.05%, 29.05%, and 53.79%, respectively, which implied that cation exchange played the second important role for Mn^{2+} adsorption. The surface complexation and chelation with cation-π merely contributed 0–0.05% and 0–2.78% of the total manganese removal, respectively.

Precipitation. A comparison of SEM images of biochar before (Fig. 2) and after (Fig. S2†) the adsorption of Mn^{2+}, indicated the occurrence of an intuitive and obvious precipitation phenomenon. The results showed that particles precipitated during the adsorption process were dispersed on the surfaces of BC and Pre-BC. However, the particles formed by precipitating of Post-BC with relatively low adsorption capacity were hardly noticeable. In order to demonstrate the type of precipitation, an XPS analysis was conducted. According to the XPS refined scan spectra of Mn 3s after adsorption (Fig. S3†), the peak intervals of 5.75 eV in BC, 5.63 eV in Pre-BC and 5.65 eV in Post-BC represent the existence of Mn^{2+},[39] and the occupation percentages of the total manganese content were 89.69%, 83.77%, and 100%, respectively. These results suggested that most of the manganese was adsorbed onto the biochar and remained in the divalent state, a similar phenomenon observed in a previous study.[22] The peak intervals of 3.39 eV in BC and 3.45 eV in Pre-BC represented the MnO_2 fines,[39] which contributed to the remaining small part of the adsorption capacity. The previous study had revealed that carbonates and silicates might play roles in metal ion adsorption on biochar.[23,24] As shown in Fig. S4,† divalent manganese was detected as $MnCO_3$ contributing to the adsorption function of precipitation, which could be proved by the Mn 2p 2p3 peaks of 644.86 eV in BC, 644.62 eV in Pre-BC, and 646.04 eV in Post-BC.[22] The precipitation of $MnCO_3$ contribute to 27.27%, 33.33%, and 38.83% in BC, Pre-BC, and Post BC, respectively. Residual divalent manganese formed by precipitation could be ascribed to silicate precipitation. It has been reported that silicon-rich biochar from rice straw would easily form silicate-like precipitates during the adsorption process of heavy metals.[40,41] As depicted in the Na 1s refined spectrum of XPS shown in Fig. S5,† the peaks at 1072.20 eV in BC, 1072.37 eV in Pre-BC, and 1072.90 eV in Post-BC are represented by $Na_2(AlSi_3O_8)$, $Na_2Al_2Si_3O_{10} \cdot 2H_2O$, and $Na(AlSi_2O_6) \cdot H_2O$, respectively.[42] After adsorption, the peaks disappeared, suggesting that these silicon-containing functional groups formed new precipitates with Al–Si–O–Mn. Due to the possibility of tiny Mn^{2+} being oxidized under the
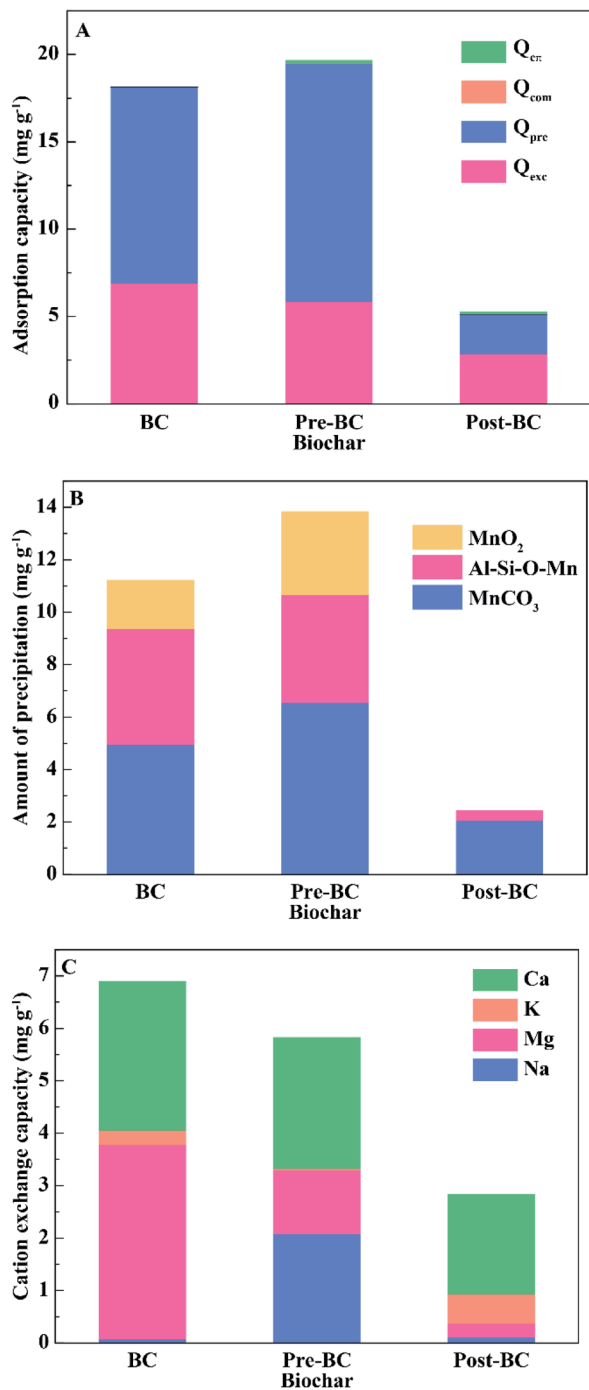
Fig. 5 Screening adsorption functions on manganese removal by BC, Pre-BC, Post-BC. (A) Adsorption capacity of different adsorption functions. (B) Amount of precipitation of different particles. (C) Cation exchange capacity of different cations.

experimental operation, a small redox Mn(II) with the addition of biochar during the adsorption process might have occurred, as shown in the Mn 3s spectra (Fig. S3†). Such a phenomenon was also observed in a previous study.[43,44]

As shown in Fig. 5A, the alkali pre-modification increased the amount of precipitation, while the alkali post-modification decreased compared to the pristine biochar. This phenomenon

was due to their different physicochemical properties responsible for forming precipitation. The types of precipitated particles indicated that carbonate and Si were correlated with the adsorption force of precipitation. As shown in Fig. 5B, the formation of $MnCO_3$ could be ascribed to the precipitation, which was similarly approved by the removal of lead by using alkali lignin-derived biochar.[19] The amount of carbonate formation in BC, Pre-BC, and Post-BC was 4.95, 6.56, and 2.05 mg g^{-1} (Fig. 5B), respectively. The intensity of carbonate peaks in the FTIR spectrum followed the order Pre-BC > BC > Post-BC (Fig. 1), which indicated that alkali pre-modification enhanced the adsorption performance of Mn^{2+} by increasing the carbonate concentration in biochar. Additionally, the amounts of $Al–Si–O^{x-}$ formed in BC, Pre-BC, and Post-BC were 4.42, 4.09, and 0.39 mg g^{-1} (Fig. 5B), respectively, which matched with the sequence of Al and Si contents as BC > Pre-BC > Post-BC (Table 1). The elemental distribution in the XPS spectrum before and after adsorption was analysed. As displayed in Fig. 6A and B, the Si content was basically unchanged for BC and Pre-BC with the formation of Al–Si–O–Mn particles. However, the Si content was significantly decreased for Post-BC, which might result in the difficulty of forming similar precipitation particles (Fig. 6C). Therefore, the biochar prepared using the oxygen-limited pyrolysis process could fix silicon and aluminum to promote the adsorption of Mn^{2+}. However, the alkali post-modification would wash away some of the minerals and reduced the stability of the combination between silica-alumina and biochar.

The amounts of the formed precipitate by MnO_2 for BC and Pre-BC were 1.87 and 3.19 mg g^{-1}, respectively, while Post-BC displayed less formation capacity (Fig. 5B). The formation of a small amount of MnO_2 could be ascribed to the turbulence of the liquid during experimental operation since oxygen might dissolve in the liquid during agitation.[44]

Cation exchange. Cation exchange is considered the main function for heavy metal adsorbing by biochar.[19] As shown in Fig. 6, the weight % of Na, Mg, K, and Ca on the surface of biochar decreased significantly, matching the increase in Mn contents after adsorption. These results suggested that the cation ions bound to the functional groups on biochar could undergo displacement with Mn^{2+}. The sequence of total cation exchange capacity of different was BC > Pre-BC > Post-BC (Fig. 5C), which could be ascribed to the sum content of Na, Mg, K, and Ca in the biochar (Table 1). The outcome suggested that the more exchangeable cations contained in the biochar, displaying the higher the cation exchange capacity.

It should be noted that the same ions of Na, Mg, K, and Ca displayed different exchange capacities in different biochars. As shown in Fig. 5C, the cation exchange of BC was mainly contributed by Mg^{2+} and Ca^{2+}. As for Pre-BC, Mg^{2+}, Na^+ and Ca^{2+} played significant roles in the exchange with Mn^{2+}. It was observed that Ca^{2+} was predominant for the cation exchange in Post-BC. This discrepancy among different biochar was attributed to the affinities between biochars and cations.

Surface complexation. The demineralized biochar showed limited adsorption capacity for Mn^{2+}, as shown in Fig. 5A, which indicated that the function of the surface complexation could
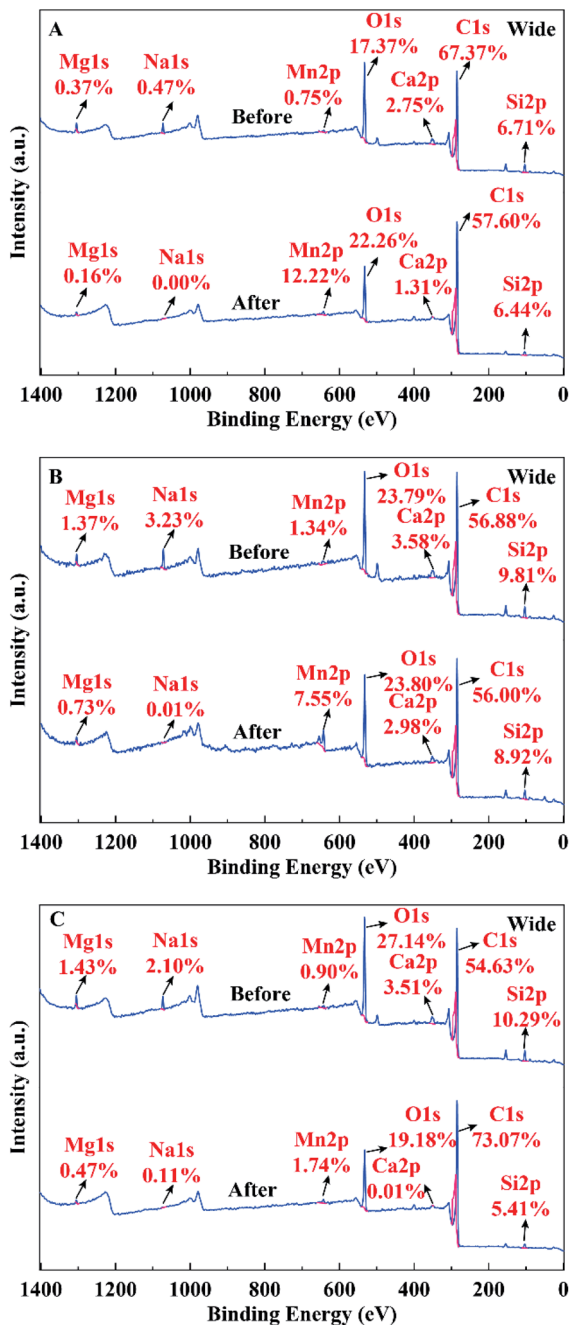
Fig. 6 XPS spectra before and after adsorption. (A) BC, (B) Pre-BC, (C) Post-BC.

be ignored in this study. The pH hardly changed during the adsorption of demineralized biochar (Table S1†), and the calculated value of the surface complexation function was close to zero. The adsorption of Mn^{2+} was hardly proceeded by surface complexation, which implied that Mn^{2+} was less likely to bind to the acidic oxygen-containing functional groups.[44,45]

Chelation with cation-π. With regard to the chelation with cation-π, the amount was determined as shown in Fig. 5A. The values for BC, Pre-BC, and Post-BC were 0, 0.19, and 0.15 mg g^{-1}, contributing 0%, 0.97%, and 2.78% of the total Mn^{2+}

removal, respectively. It has been reported that Mn^{2+} is difficult to chelate with cation-π of the aromatic functional groups on the surface of biochar.[45] Therefore, less amount of Mn^{2+} was detected to be adsorbed on biochar through chelation with cation-π interactions in this study, as shown in Fig. 5A.

Conclusions

The existence of manganese ions in the drinking water reservoirs could pose potential threats to human health. In this study, biochar modified with alkali was applied to remove Mn^{2+} from water. Compared with the pristine biochar, alkali pre-modification biochar showed higher adsorption capacity and faster adsorption velocity, which could be used as an applicable material for Mn^{2+} removal from lakes and reservoirs. The maximum adsorption capacities for BC, Pre-BC, and Post-BC were 20.59, 28.37, and 8.06 mg g^{-1}, respectively. The Langmuir isotherm model and the pseudo-second-order kinetic model were suitable fitting models to describe the adsorption process. It was revealed that the adsorption of Mn^{2+} by biochar was mainly contributed by cation exchange and precipitation. The precipitation of manganese minerals onto BC, Pre-BC, and Post-BC accounted for 62.95%, 69.35%, and 43.38%, of the total removal amount, and cation exchange accounted for 38.05%, 29.65%, and 53.79%, respectively, of the total. With regard to precipitation, the formation of $MnCO_3$ and Al–Si–O–Mn was mainly driven by the precipitation of Mn^{2+} on the biochar surface. Alkali and alkaline earth metals facilitated the behavior of cation exchange, where the primary contributing ions for cation exchange were Na^+, Mg^{2+} and Ca^{2+} during the adsorption process. The research outcomes were expected to provide methodological support for controlling manganese endogenous pollution for a safe drinking water supply.

Author contributions

Jie Zhao: conceptualization, methodology, formal analysis, investigation, data curation, writing-original draft. Zhi-long Ye: project administration, funding acquisition, supervision, writing-review and editing. Xiaofang Pan: reviewing and editing. Guanjing Cai: methodology and software. Jiani Wang: formal analysis.

Conflicts of interest

The authors declare that they have no known competing financial interests or personal relationships that could have appeared to influence the work reported in this paper.

Acknowledgements

References

1 E. Bertone, R. A. Stewart, H. Zhang, M. Bartkow and C. Hacker, *Environ. Model. Software*, 2015, **73**, 133–147.

2 F. O. Ossa, A. Hofmann, J. E. Spangenberg, S. W. Poulton, E. E. Stueken, R. Schoenberg, B. Eickmann, M. Wille, M. Butler and A. Bekker, *Proc. Natl. Acad. Sci. U. S. A.*, 2019, **116**, 6647–6652.

3 Y. Chen, J. Long, S. Chen, Y. Xie, Z. Xu, Z. Ning, G. Zhang, T. Xiao, M. Yu, Y. Ke, L. Peng and H. Li, *Sci. Total Environ.*, 2022, **805**, 150237.

4 H. Yang, X. Tang, X. Luo, G. Li, H. Liang and S. Snyder, *J. Hazard Mater.*, 2021, **415**, 125707.

5 Q. An, C. Zhang, B. Zhao, Z. Li, S. Deng, T. Wang and L. Jin, *Sci. Total Environ.*, 2021, **793**, 148609.

6 A. D. Zand and M. R. Abyaneh, *Sustain. Environ. Res.*, 2020, **30**, 18.

7 M. A. Embaby, S. M. Abdel Moniem, N. A. Fathy and A. A. El-Kady, *Heliyon*, 2021, **7**, e08218.

8 A. E. B. Mahdavi, E. Panahpour, R. J. Kalbasi and A. Gholami, *Desalination Water Treat.*, 2021, **210**, 316–329.

9 Y. Gao, X. Zhu, Q. Yue and B. Gao, *J. Environ. Sci.*, 2018, **73**, 185–194.

10 D. B. Pal, A. Singh, J. M. Jha, N. Srivastava, A. Hashem, M. A. Alakeel, E. F. Abd Allah and V. K. Gupta, *Bioresour. Technol.*, 2021, **339**, 125606.

11 H. Lu, L. Hu, W. Zheng, S. Yao and L. Qian, *J. Cleaner Prod.*, 2020, **262**, 121479.

12 X. Fan, J. Zhang, Y. Xie, D. Xu, Y. Liu, J. Liu and J. Hou, *Water Sci. Technol.*, 2021, **83**, 1429–1445.

13 K. Luo, Y. Pang, D. Wang, X. Li, L. Wang, M. Lei, Q. Huang and Q. Yang, *J. Environ. Sci.*, 2021, **108**, 201–216.

14 C. Wu, L. Li, H. Zhou, J. Ai, H. Zhang, J. Tao, D. Wang and W. Zhang, *J. Environ. Sci.*, 2021, **100**, 340–352.

15 H. Chen, F. Xu, Z. Chen, O. Jiang, W. Gustave and X. Tang, *J. Environ. Sci.*, 2020, **96**, 186–193.

16 B. Hu, Y. Ai, J. Jin, T. Hayat, A. Alsaedi, L. Zhuang and X. Wang, *Biochar*, 2020, **2**, 47–64.

17 W. H. Huang, D. J. Lee and C. Huang, *Bioresour. Technol.*, 2021, **319**, 124100.

18 L. Sui, C. Tang, Q. Du, Y. Zhao, K. Cheng and F. Yang, *J. Environ. Sci.*, 2021, **106**, 116–123.

19 F. Wu, L. Chen, P. Hu, Y. Wang, J. Deng and B. Mi, *Bioresour. Technol.*, 2021, **322**, 124539.

20 L. Wang, Y. Wang, F. Ma, V. Tankpa, S. Bai, X. Guo and X. Wang, *Sci. Total Environ.*, 2019, **668**, 1298–1309.

21 A. Peter, B. Chabot and E. Loranger, *J. Environ. Manage.*, 2021, **290**, 112569.

22 Q. An, Y. Miao, B. Zhao, Z. Li and S. Zhu, *Mater. Chem. Phys.*, 2020, **248**, 122895.

23 X. Cui, S. Fang, Y. Yao, T. Li, Q. Ni, X. Yang and Z. He, *Sci. Total Environ.*, 2016, **562**, 517–525.

24 L. Y. Gao, J. H. Deng, G. F. Huang, K. Li, K. Z. Cai, Y. Liu and F. Huang, *Bioresour. Technol.*, 2019, **272**, 114–122.

25 Z. Wang, G. Liu, H. Zheng, F. Li, H. H. Ngo, W. Guo, C. Liu, L. Chen and B. Xing, *Bioresour. Technol.*, 2015, **177**, 308–317.

26 A. Li, Y. Zhang, W. Ge, Y. Zhang, L. Liu and G. Qiu, *Bioresour. Technol.*, 2021, **347**, 126425.

27 K. Iamsaard, C. H. Weng, L. T. Yen, J. H. Tzeng, C. Poonpakdee and Y. T. Lin, *Bioresour. Technol.*, 2022, **344**, 126131.

28 Y. Xu and B. Chen, *J. Soils Sediments*, 2015, **15**, 60–70.

29 Z. Z. Chowdhury, M. R. Hasan, S. B. Abd Hamid, E. M. Samsudin, S. M. Zain and K. Khalid, *RSC Adv.*, 2015, **5**, 6345–6356.

30 J. Kończyk, K. Kluziak and D. Kołodyńska, *J. Environ. Manage.*, 2022, **313**, 114958.

31 L. Gao, Z. Li, W. Yi, L. Wang, P. Zhang, Z. Wan and Y. Li, *J. Cleaner Prod.*, 2021, **325**, 129328.

32 U. Tyagi, *Bioresour. Technol.*, 2022, **345**, 126475.

33 A. Youngwilai, P. Kidkhunthod, N. Jearanaikoon, J. Chaiprapa, N. Supanchaiyamat, A. J. Hunt, Y. Ngernyen, T. Ratpukdi, E. Khan and S. Siripattanakul-Ratpukdi, *Sci. Total Environ.*, 2020, **713**, 136708.

34 J. Chwastowski, D. Bradło and W. Żukowski, *Materials*, 2020, **13**, 2782.

35 Y. S. Ho, *J. Hazard Mater.*, 2006, **136**, 681–689.

36 H. Qiu, L. Lv, B. C. Pan, Q. J. Zhang, W. M. Zhang and Q. X. Zhang, *J. Zhejiang Univ., Sci., A*, 2009, **10**, 716–724.

37 G. M. Al-Senani and F. F. Al-Fawzan, *Egypt. J. Aquat. Res.*, 2018, **44**, 187–194.

38 H. N. Tran, S. J. You, A. Hosseini-Bandegharaei and H. P. Chao, *Water Res.*, 2017, **120**, 88–116.

39 M. C. Biesinger, B. P. Payne, A. P. Grosvenor, L. W. M. Lau, A. R. Gerson and R. S. C. Smart, *Appl. Surf. Sci.*, 2011, **257**, 2717–2730.

40 Y. H. Fei, Z. Zhang, Z. Ye, Q. Wu, Y. T. Tang and T. Xiao, *J. Environ. Sci.*, 2022, **113**, 64–71.

41 F. Huang, L. Y. Gao, R. R. Wu, H. Wang and R. B. Xiao, *Sci. Total Environ.*, 2020, **731**, 139163.

42 H. Seyama and M. Soma, *J. Chem. Soc. Faraday Trans. I*, 1985, **81**, 485–495.

43 Z. Fan, Q. Zhang, M. Li, W. Sang, Y. Qiu, X. Wei and H. Hao, *J. Cleaner Prod.*, 2020, **256**, 120672.

44 M. Idrees, S. Batool, H. Ullah, Q. Hussain, M. I. Al-Wabel, M. Ahmad, A. Hussain, M. Riaz, Y. S. Ok and J. Kong, *J. Mol. Liq.*, 2018, **266**, 373–380.

45 H. Yankovych, V. Novoseltseva, O. Kovalenko, D. M. Behunova, M. Kanuchova, M. Vaclavikova and I. Melnyk, *J. Environ. Manage.*, 2021, **292**, 112757.